Supporting information of "Characterization of submicron aerosols influenced by biomass burning at a site in the Sichuan Basin, southwestern China"

Wei Hu, Min Hu[*], Weiwei Hu, Hongya Niu, Jing Zheng, Yusheng Wu, Wentai Chen, Chen Chen, Lingyu Li, Min Shao,

Shaodong Xie, Yuanhang Zhang

State Key Joint Laboratory of Environmental Simulation and Pollution Control, College of Environmental Sciences and

Engineering, Peking University, Beijing 100871, China

Correspondence to: M. Hu (minhu@pku.edu.cn)

1 **Table S1** Average concentrations and fractions of chemical species in submicron aerosols in different sites in China. The numbers in parenthesis are the

2 proportions of chemical components in PM$_1$. The O/C and H/C ratios of OA are corrected herein by the "Improved-Ambient" method (Canagaratna et al., 2015).

3 Unit of mass concentrations: µg m^{-3}. *The two factors are defined as OOA-1 and OOA-2; [#], [+] and [≠] are factors defined as OOA, COA and CCOA, respectively.

4 [a] data are not corrected by the "Improved-Ambient" method.

	Ziyang (This study)					Beijing[1]	Shanghai[2]	Shenzhen[3,4]		Jiaxing[5]		Heshan[6]	Kaiping[7]	Backgarden[8]	Changdao Island[9]
Site type	Suburban					Urban				Suburban/Rural				Coastal/ Background	
Sampling time	Overall	P1	P2	C	P3	Summer	Summer	Summer	Autumn	Summer	Winter	Autumn	Autumn	Summer	Spring
RH (%)	80	91	86	24	57	67	66	73	63	73	65	67	69	78	56
T (°C)	8	11	10	7	4	28	21	29	20	29	9	20	24	29	8
PM$_1$	59.7	91.6	71.8	7.6	56.9	63.1	29.2	51.1	44.5	32.9	41.9	47.9	33.1	35.4	46.6
Organics	21.5(36)	31.7(35)	25.6(36)	2.9(38)	23.8(42)	23.9(38)	8.4(29)	19.4(38)	17.7(40)	10.6(32)	12.7(30)	17.4(36)	11.2(34)	13.4(38)	13.4(30)
LV-OOA	7.5(13)	16.3(18)	10.4(15)	0.04(0.5)	5.5(10)	8.1(13)*	2.4(8)	5.6(11)	4.9(11)	7.2(22)[#]	3.8(9)[#]	6.8(14)	4.0(12)	5.1(14)	6.1(13)
SV-OOA	7.9(13)	4.6(5)	9.1(13)	1.8(23)	7.1(12)	5.7(9)*	3.9(14)	7.7(15)	3.3(8)			5.0(10)	4.4(13)	3.8(11)	3.3(7)
HOA	3.2(5)	6.3(7)	3.5(5)	0.6(8)	5.2(9)	4.3 (7)	2.0(7)	6.1(12)	5.2(12)	3.3(10)	5.0(12)	3.1(6)		4.6(13)	3.2(7)
BBOA	3.0(5)	4.5(5)	2.6(4)	0.5(7)	6.1(11)	5.8 (9)[+]			4.3(10)		3.8(9)	2.5(5)	2.7(8)		1.2(3) [≠]
Sulfate	11.7(20)	15.5(17)	14.6(20)	2.1(28)	8.2(14)	16.8(27)	9.7(33)	19.0(37)	10.9(25)	8.3(25)	7.1(17)	10.0(21)	11.2(34)	12.5(35)	8.3(19)
Nitrate	9.4(16)	17.5(19)	12.1(17)	0.5(6)	6.1(11)	10.0(16)	4.8(16)	3.0(6)	4.5(10)	5.9(18)	7.5(18)	6.2(13)	3.5(11)	1.3(4)	12.2(28)
Ammonium	8.3(14)	12.7(14)	9.8(14)	1.0(14)	6.6(12)	10.0(16)	3.9(13)	6.1(12)	4.5(10)	4.1(13)	4.9(12)	4.6(10)	4.6(14)	4.1(12)	6.5(15)
Chloride	2.3(4)	2.8(3)	2.2(3)	0.3(3)	4.0(7)	0.5(1)	0.5(2)	0.3(1)	0.7(2)	1.0(3)	2.7(7)	1.5(3)	0.4(1)	0.5(2)	1.3(3)
BC	6.5(11)	11.3(12)	7.6(11)	0.8(11)	8.2(14)	1.8(3)	2.0(7)	3.4(7)	6.2(14)	3.0(9)	7.1(17)	8.2(17)	2.2(7)	3.5(10)	2.5(6)
OOA/OA (%)	71	66	78	61	52	58	76	68	48	69	30	67	74	66	67
OM/OC	2.02	2.03	2.08	1.76	1.85		1.55[a]		1.71	1.67	1.75	1.87	1.94		1.91[a]
O/C	0.65	0.65	0.69	0.46	0.52	0.41	0.40		0.39	0.36	0.43	0.50	0.60		0.59[a]
H/C	1.56	1.58	1.55	1.50	1.60	1.63	1.92		1.83	1.94	1.73	1.63	1.64		1.33[a]
$\overline{OS_C}$	-0.26	-0.28	-0.17	-0.59	-0.57	-0.81	-1.12		-1.04	-1.22	-0.87	-0.63	-0.44		-0.15[a]

5 References: 1. Huang et al., 2010; 2. Huang et al., 2012; 3. Gong et al., 2013; 4. He et al., 2011; 5. Huang et al., 2013; 6. Gong et al., 2012; 7. Huang et al.,

6 2011; 8. Xiao et al., 2011; 9. Hu et al., 2013.

S1 Location of the observation site
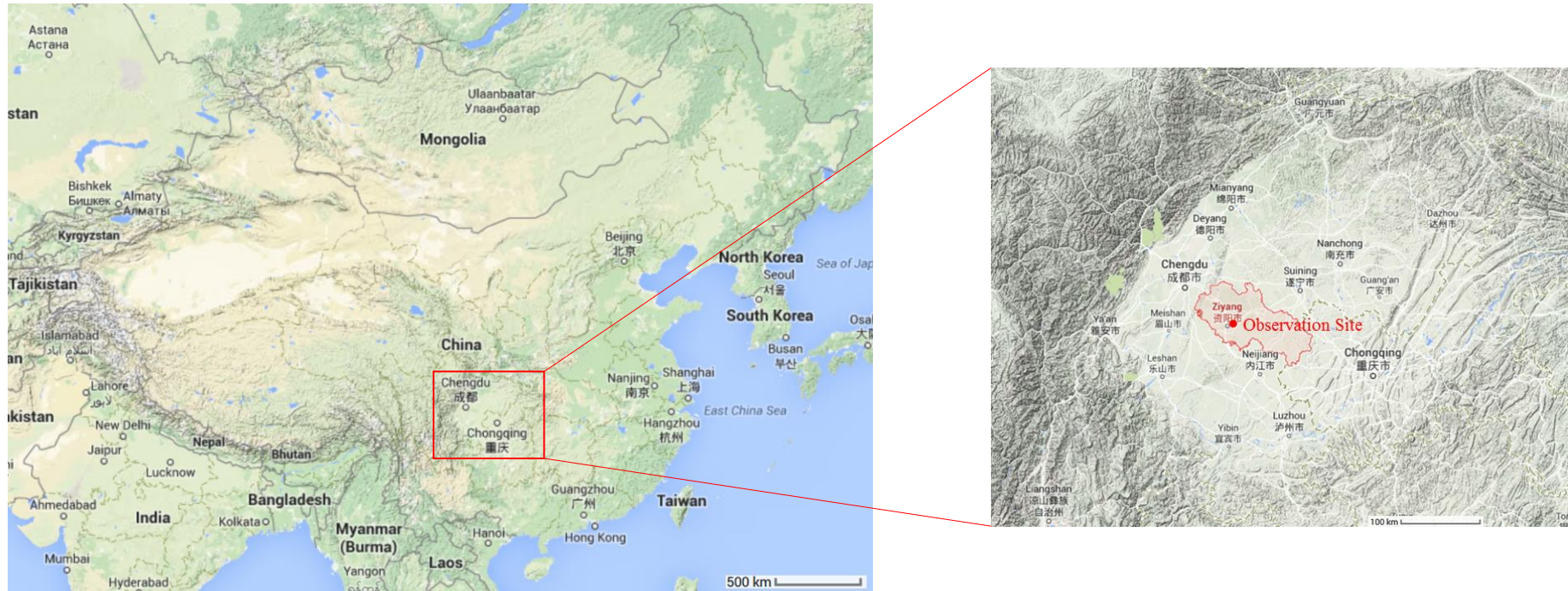
Figure S1. Location of the observation site in Ziyang in the Sichuan Basin. The topography of the Sichuan Basin is also shown (from Google Map).

S2 Backward trajectory of air parcels

The backward trajectories of air parcels during the campaign were calculated by NOAA's HYSPLIT4.9 model (www.arl.noaa.gov/hysplit.html). The total run time and height of start locations were set as 72 hours and 500 m, respectively. The result of backward trajectory clustering is shown in Fig. 1.

The climate and weather in the Sichuan Basin are relatively isolated. During the one-month long campaign, only in one day, 29 December, it was affected by the invasion of long-transported air mass from Northwest China accompanying with strong wind. In all the rest days, the air parcels were lingering in the basin due to the block of special basin terrain, and the atmospheric processes are dominated by the separate meteorology of the basin. Therefore, the pollutants in Sichuan Basin are difficult to diffuse in the static air. Local pollution is dominated in this region, while long-distance transportation has little impact.

S3 Determination of the PMF solution

Factor number from 1 to 10 and the different seeds (0-50) were selected to run in the model. A 4-factor solution was selected for the final results. Four PMF OA factors are semi-volatile oxygenated OA (SV-OOA; O/C=0.73), low-volatility oxygenated OA (LV-OOA; O/C=1.02), biomass burning OA (BBOA; O/C =0.32) and hydrocarbon-like OA (HOA, O/C =0.10). The performances of spectra and time series of the four factors at different f_{peak} were also investigated. The detailed information on how to select PMF factors can be found in Figure S2-S3 and Table S2-S4.
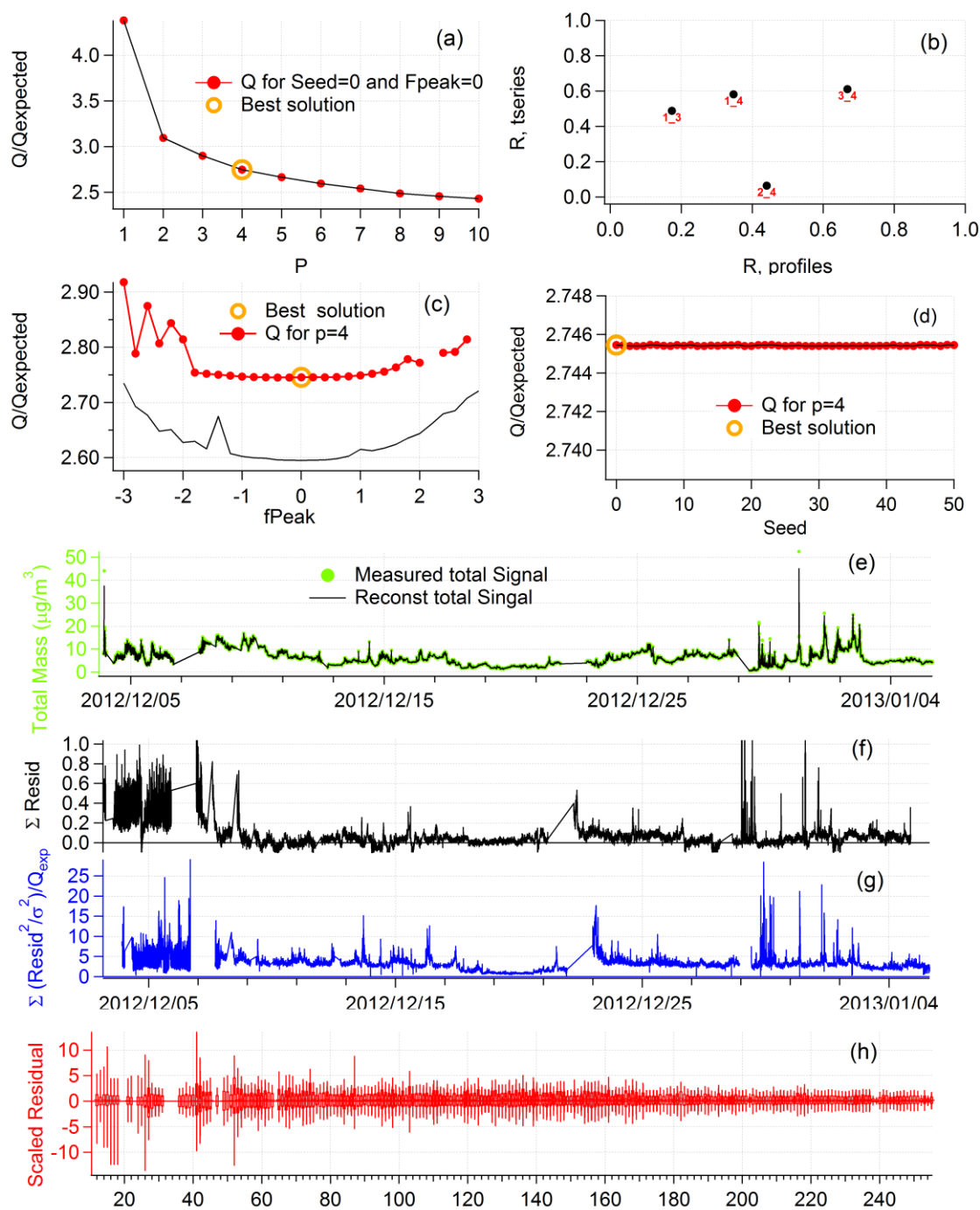
Figure S2 Diagnostics plots of PMF analysis on OA mass spectral matrix. Very stable PMF solution among

different seed numbers (0-50) was also found, which suggests the PMF solution is robust here.
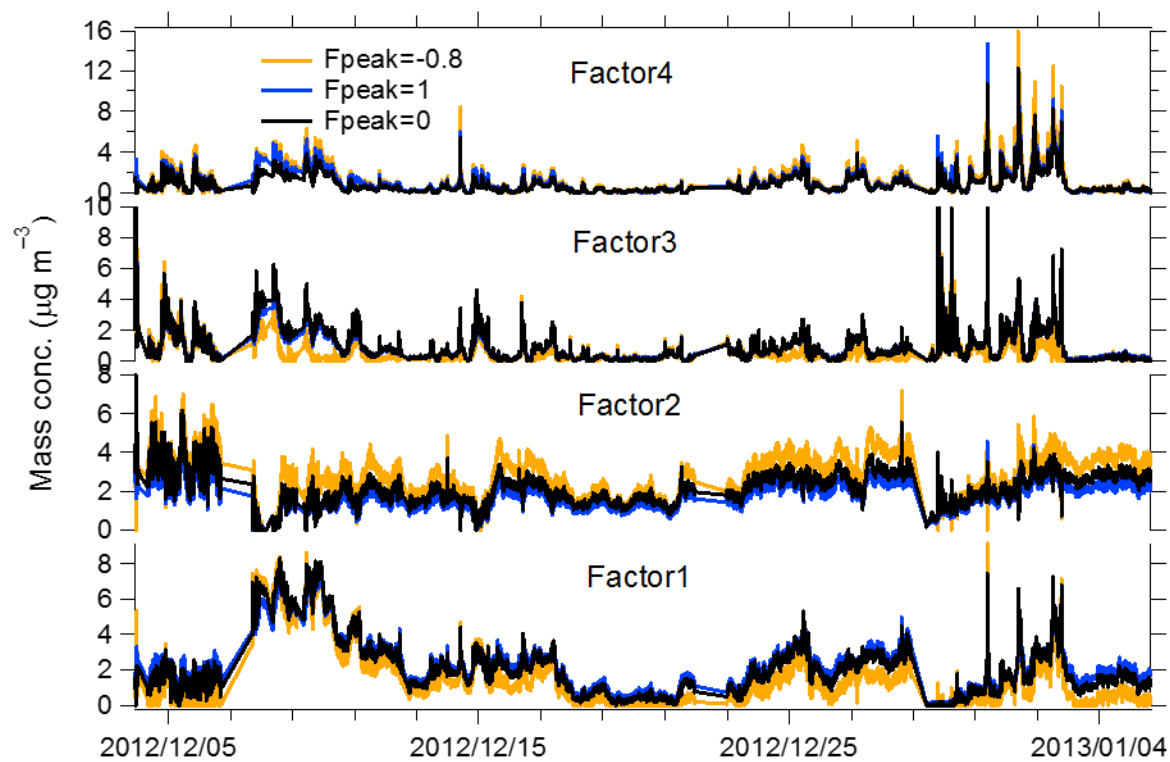
2 **Figure S3.** The spectra and time series of 4-factor solution at different f_{peak} values.

1 **Table S2** Descriptions of PMF solutions obtained at Ziyang site.

Factor number	Fpeak	Seed	Q/Q$_{exp}$	Solution Description
1	0	0	4.38	Too few factors, large residuals at time periods and key m/z's
2	0	0	3.10	Too few factors, large residuals at time periods and key m/z's
3	0	0	2.90	Too few factors (OOA-, HOA- and BBOA-like). The Q/Q$_{exp}$ at different seeds (0-50) are very unstable. Factors are mixed to some extend based on the time series and spectra.
4	**0**	**0**	**2.75**	**Optimum choices for PMF factors (LV-OOA, SV-OOA, HOA and BBOA). Time series and diurnal variations of PMF factors are consistent with the external tracers. The spectra of four factors are consistent with the source spectra in AMS spectra database.**
5-10	0	0	2.66-2.43	Factor split. Take 5 factor number solution as an example, LV-OOA was split into two factors with similar spectra, however, different time series. When factor num. = 6, there is extra split factor from BBOA.
4	-3 to 3	0	2.75-2.92	In FPEAK range from −0.8 to1.0, factor MS and time series are nearly identical.

Table S3 The uncentered correlation coefficients between the MS of OA factors resolved in this study and the average MS of OA factors.

	Ziyang				Average						
	LV-OOA	SV-OOA	HOA	BBOA	LV-OOA	SV-OOA	HOA	BBOA	CCOA	COA	Vehicle-OA
LV-OOA	1.00				0.99	0.92					
SV-OOA	0.98	1.00			0.99	0.97					
HOA	0.38	0.52	1.00				0.96	0.89	0.65	0.96	0.88
BBOA	0.48	0.59	0.88	1.00			0.86	0.93	0.65	0.81	0.68

Note: The average MS of OA factors are summarized by Hu (2012). The MS of OA factors resolved in studies over China are from He et al. (2010, 2011), Hu et al. (2013, 2016) and Huang et al. (2010, 2011). Other MS of OA factors are from AMS Spectral Database (Unit Mass Resolution). Specifically, the published spectra used for the average MA of each OA factor are listed as follows. **LV- and SV-OOA:** He et al., 2011; Hu et al., 2016; Huang et al., 2011. **HOA:** Aiken et al., 2009; He et al., 2011; Hu et al., 2016. **BBOA:** Aiken et al., 2009; He et al., 2010, 2011; Huang et al., 2011; Lanz et al., 2008; Ng et al., 2010; Weimer et al., 2008; **COA:** He et al., 2010; Hu et al., 2016; Huang et al., 2010; Mohr et al., 2009; **CCOA:** Hu et al., 2013; Vehicle-OA: Canagaratna et al., 2004; Mohr et al., 2009.

Table S4 Correlation matrix of gaseous pollutants and particulate chemical compositions in submicron aerosols.

	SO$_4^{2-}$	NO$_3^-$	NH$_4^+$	Cl$^-$	BC	C$_2$H$_4$O$_2^+$	SO$_2$	NO$_x$	NO$_y$	O$_3$	CO	Acetaldehyde	Acetonitrile	LV-OOA	SV-OOA	HOA	BBOA
SO$_4^{2-}$	1.00																
NO$_3^-$	**0.65**	1.00															
NH$_4^+$	**0.85**	**0.81**	1.00														
Cl$^-$	0.34	0.05	0.56	1.00													
BC	0.59	0.43	**0.62**	0.55	1.00												
C$_2$H$_4$O$_2^+$	0.59	0.47	0.59	0.46	**0.84**	1.00											
SO$_2$	0.18	0.01	0.32	**0.62**	0.35	0.30	1.00										
NO$_x$	0.33	0.08	0.44	**0.73**	**0.68**	0.47	0.53	1.00									
NO$_y$	0.39	0.22	0.53	**0.72**	**0.74**	0.54	0.54	**0.98**	1.00								
O$_3$	-0.44	-0.35	-0.55	-0.45	-0.48	-0.33	-0.09	-0.47	-0.46	1.00							
CO	0.46	0.08	0.53	**0.82**	0.53	0.43	0.55	**0.76**	**0.74**	-0.56	1.00						
Acetaldehyde	0.22	0.05	0.25	0.50	**0.60**	**0.64**	**0.65**	0.51	0.55	-0.04	0.50	1.00					
Acetonitrile	0.42	0.14	0.54	**0.80**	**0.74**	**0.66**	**0.61**	**0.77**	**0.79**	-0.46	**0.84**	**0.71**	1.00				
LV-OOA	**0.65**	**0.66**	**0.68**	0.22	**0.75**	**0.77**	0.10	0.31	0.39	-0.31	0.20	0.34	0.44	1.00			
SV-OOA	0.36	0.31	0.28	-0.08	0.18	0.28	0.09	-0.13	-0.09	0.08	-0.09	0.26	-0.02	0.37	1.00		
HOA	0.26	0.15	0.36	0.57	**0.73**	**0.80**	0.39	**0.62**	**0.64**	-0.32	0.49	**0.65**	**0.73**	0.53	0.01	1.00	
BBOA	0.30	0.21	0.34	0.49	**0.77**	**0.85**	0.44	0.47	0.51	-0.21	0.42	**0.77**	**0.68**	0.55	0.25	**0.78**	1.00

Note: Correlation coefficients higher than 0.60 are in bold.

S4 Diurnal patterns of chemical species in PM$_1$ and gaseous pollutants

The diurnal patterns of main chemical components in submicron aerosols in Ziyang were shown in Fig. S4. The diurnal patterns of organics and BC were more obvious than those of other species. Both of them showed two peaks appearing in the morning (about 9:00-10:00 local time, LT) and evening (about 20:00 LT). The concentration of organics may be elevated with local primary sources, such as emissions from vehicle, biomass burning and coal combustion, as well as secondary formation. The diurnal variations of specific factors contributed to organic aerosols are as refer to Sect. 3.2. The concentration of BC was enhanced daily in the two time intervals, probably caused by the contributions of primary emissions related to local residence.

The diurnal variation of nitrate also showed a weak bimodal pattern. One peak in the morning was a little later than those of organics and BC, and the other was in the evening. The concentration of nitrate was significantly affected by gas-particle partitioning. The precursors of ammonium nitrate, e.g. gaseous nitric acid and ammonia, were in favor of converting from the gaseous phase to particulate nitrate in the morning and nighttime due to lower temperature and higher humidity. In the nocturnal atmosphere, NO$_3$ and N$_2$O$_5$ radicals, constitute an important chemical system (Brown, 2003). In the cases of Beijing and Shanghai, Pathak et al. (2011) postulated that nighttime enhancement of nitrate was related to the heterogeneous hydrolysis of N$_2$O$_5$. Furthermore, the concentration of nitrate was reduced in the afternoon, which may not only be associated with the volatilization of nitric acid and ammonia, but also be influenced by the dilution of pollutants due to the uplift of atmospheric boundary layer (Zhang et al., 2005).

Sulfate showed no evident diurnal pattern and much more steady in the whole day, indicating the regional formation and accumulation of sulfate. According to the effect of neutralization, the diurnal variation of ammonium should be of comprehensive characteristics of sulfate and nitrate. However, the pattern of ammonium was not so obvious and much more like that of sulfate. The diurnal variation of chloride was opposite to that of atmospheric temperature for its semi-volatility as ammonium chloride, with higher concentrations in the nighttime. In

addition, it was mostly emitted from combustion processes for the similar diurnal patterns with primary source tracers, such as SO_2 and CO (Zhang et al., 2005; Hu et al., 2012).
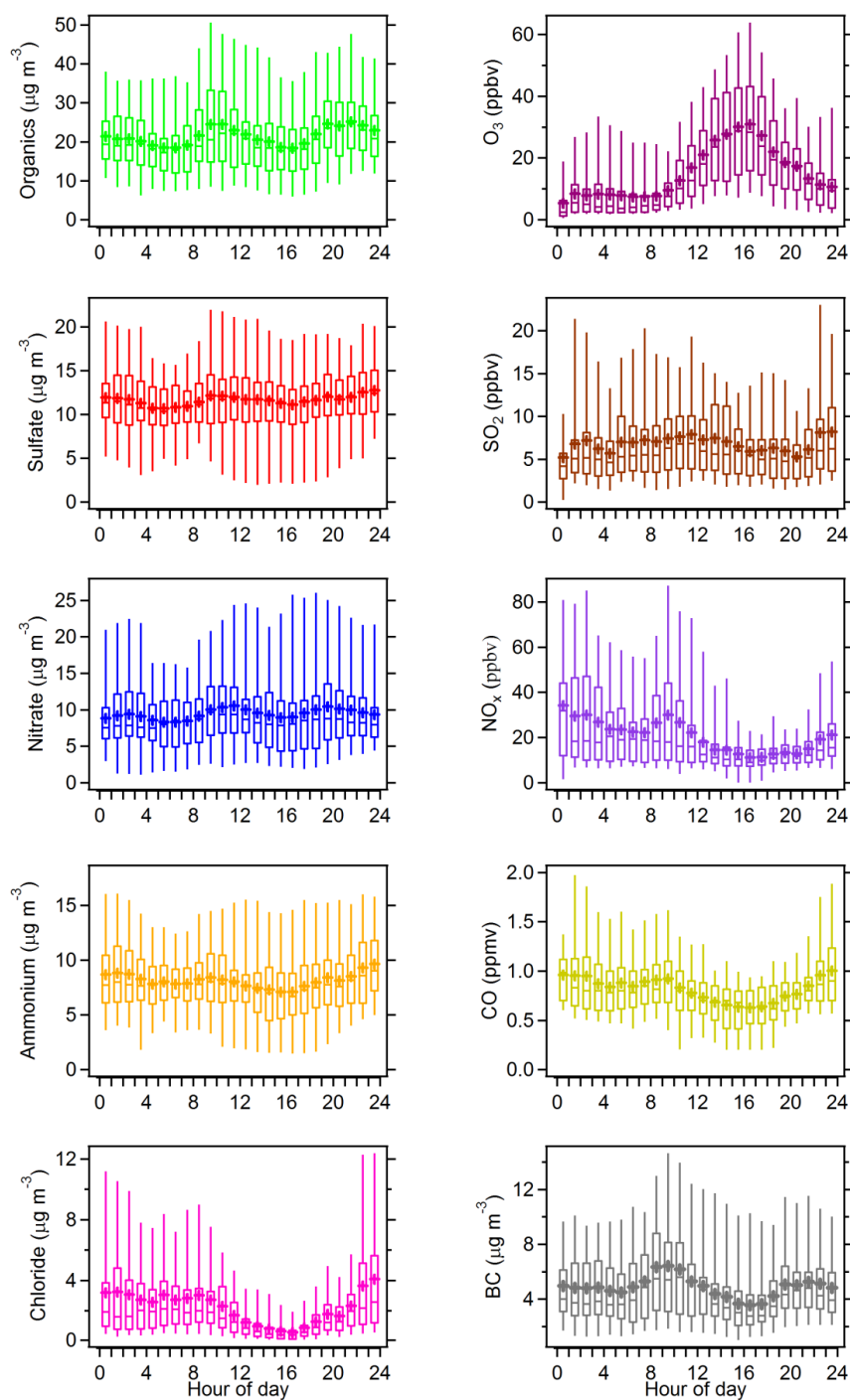
Figure S4. Diurnal patterns of chemical species of submicron particles and gaseous pollutants at Ziyang site.

S5 Morphology, mixing state and elemental compositions of particles

Atmospheric particles at Ziyang site were collected in several days. Here several groups of samples collected in foggy and hazy days, 21-22 December 2012, were chosen for preliminary illustration the properties of single particles by using TEM-EDX. The RH began to decrease from saturated (100%) to unsaturated (66%) in the afternoon of 21 December (Fig. 1a). The samples of the first group were collected in this process and the rest samples were collected in unsaturated humidity conditions, and the sampling time for each sample was 30 seconds. The analysis in detail will be shown in another paper. The morphology and the mixing state are shown in TEM photographs of single particles as Fig. 4a-d, and the elemental compositions for typical particles are shown in Fig. 4e.

As Fig. 3a-d shown, single particles collected in hazy days were mostly spherical and in internal mixing state, and dominated by particles marked as Type A and Type B. Both types of particles were consisted of volatile substances for their color was lightened and bubbles formed under the direct TEM detector light, i.e. electron beam damage. Therefore, they were considered to be secondary transformed in the atmosphere. The elemental compositions of 15 single particles were detected by EDX randomly (Fig. 3e). The percentages of sulfur-, chlorine- and potassium- containing particles were 93%, 40%, and 33%, indicating they may contain sulfate (Li and Shao, 2010; Ueda et al., 2011), and mixed with particles from primary sources such as coal combustion and biomass burning. In addition, some freshly emitted and aged soot aggregates (Type C) were also observed and only accounted for a small part in each sample. To our knowledge, particles of Type B were hygroscopic. After the decrease of RH, the concentration of submicron particles reduced from 69 μg m^{-3} to 39 μg m^{-3} due to the evaporation of water in hygroscopic particles such as particles of Type B (Lee et al., 2007). The particles collected at 19:30 LT shrank to smaller sizes than those collected at 14:51 LT. In general, the morphology and mixing state of particles varied not significantly during the hazy days.

S6 Secondary formation and aging process of OA
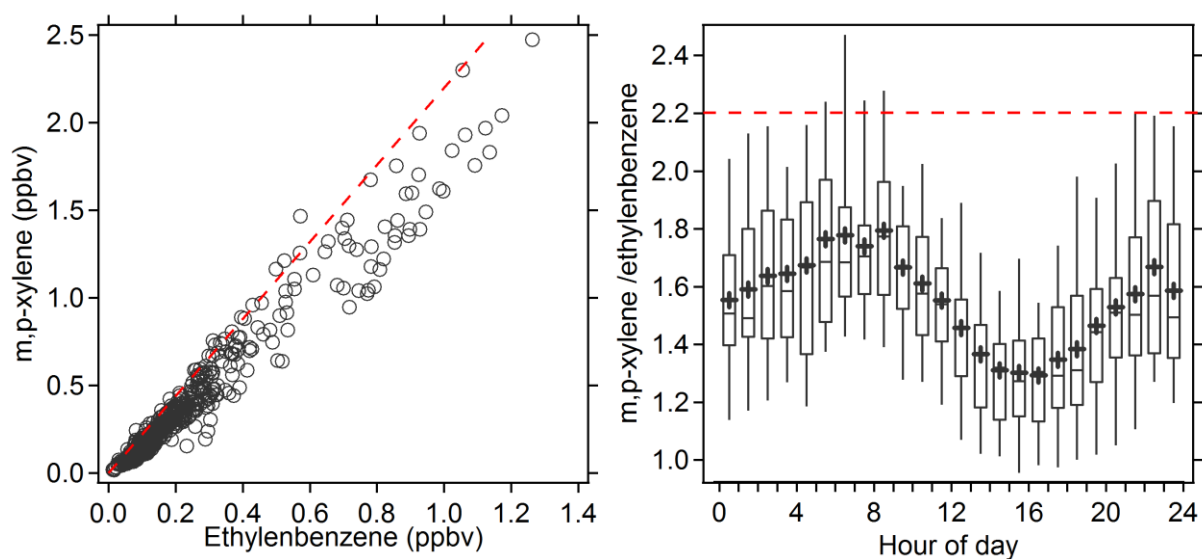
Figure S5. Correlation between m, p-xylene and ethylbenzene during the observation period at Ziyang site (left) and diurnal variation of the ratio of m, p- xylene to ethylbenzene (right). The highest ratio of m, p-xylene to benzene was about 2.2 (dash lines), which was used as the initial emission ratio of them for the calculation of photochemical age. For several data point of the ratio greater than 2.2, the calculated photochemical age less than zero were unified to zero.
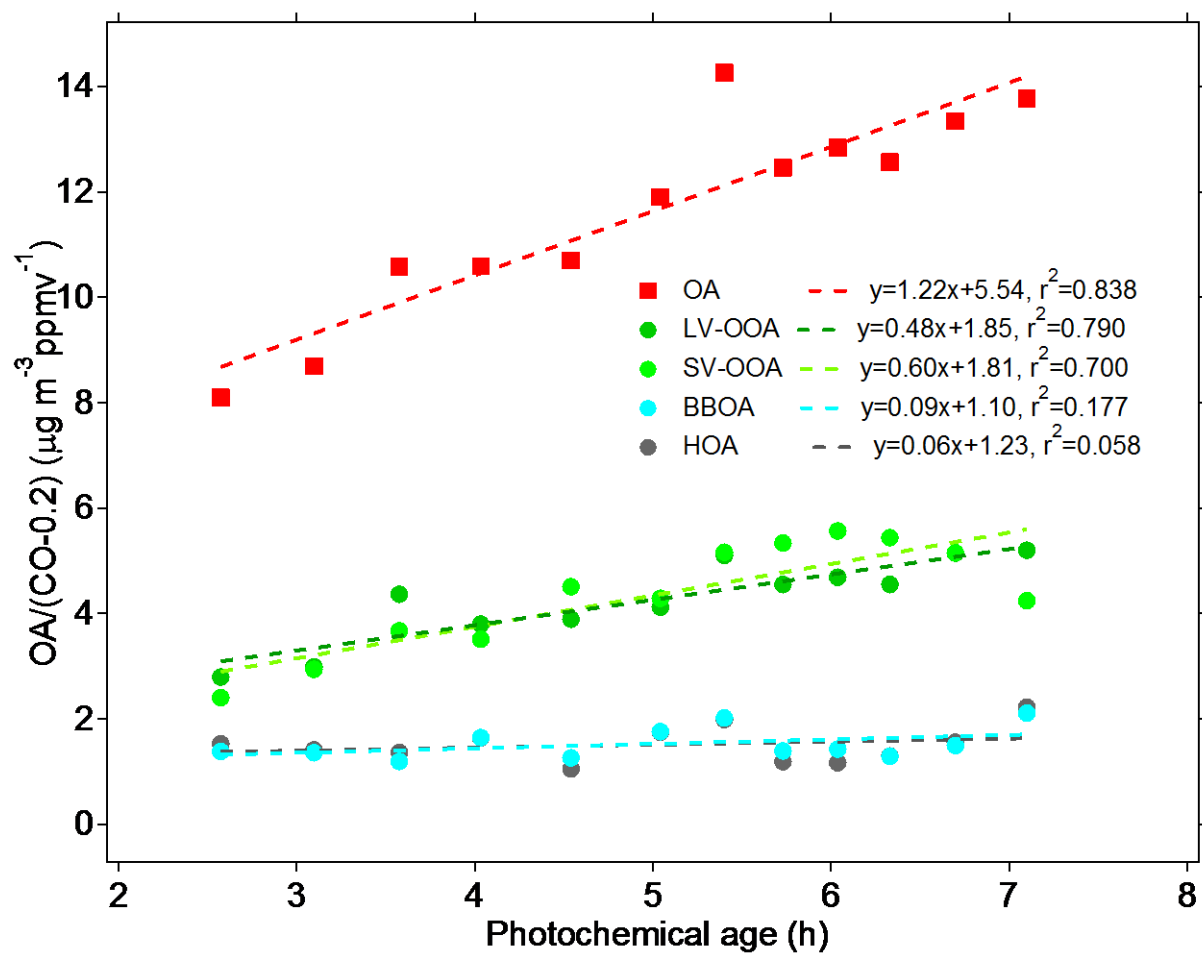
Figure S6. Variations of OA/ΔCO and PMF resolved OA factors to ΔCO with the increase of photochemical age (in the range of 2.6~7.1 hours).
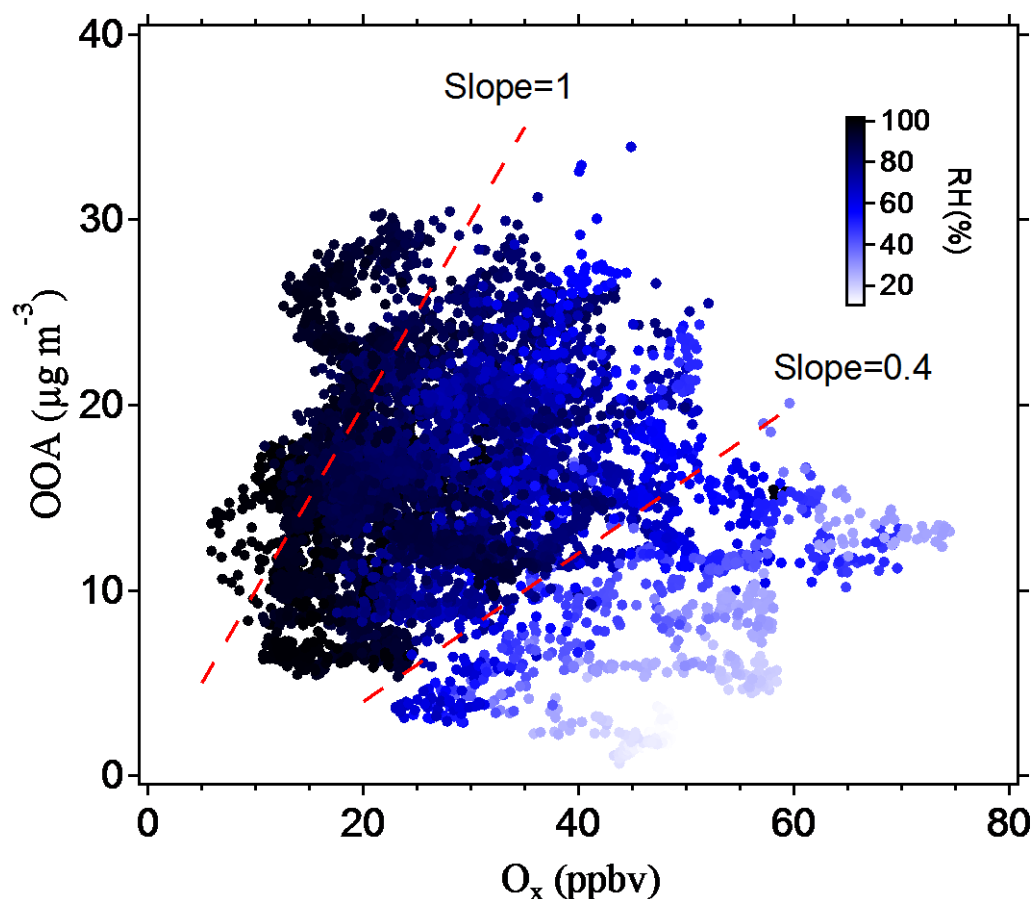
Figure S7. Scattering plot of OOA mass concentrations against O_x concentrations. Data points are color coded by RH.

References

Aiken, A. C., Salcedo, D., Cubison, M. J., Huffman, J. A., DeCarlo, P. F., Ulbrich, I. M., Docherty, K. S., Sueper, D., Kimmel, J. R., Worsnop, D. R., Trimborn, A., Northway, M., Stone, E. A., Schauer, J. J., Volkamer, R. M., Fortner, E., de Foy, B., Wang, J., Laskin, A., Shutthanandan, V., Zheng, J., Zhang, R., Gaffney, J., Marley, N. A., Paredes-Miranda, G., Arnott, W. P., Molina, L. T., Sosa, G., and Jimenez, J. L.: Mexico City aerosol analysis during MILAGRO using high resolution aerosol mass spectrometry at the urban supersite (T0) - Part 1: Fine particle composition and organic source apportionment, Atmos. Chem. Phys., 9, 6633-6653, 2009.

Brown, S. S.: Nitrogen oxides in the nocturnal boundary layer: Simultaneous in situ measurements of NO_3, N_2O_5, NO_2, NO, and O_3, J. Geophys. Res. Atmos., 108, doi: 10.1029/2002JD002917, 2003.

Canagaratna, M. R., Jayne, J. T., Ghertner, D. A., Herndon, S., Shi, Q., Jimenez, J. L., Silva, P. J., Williams, P., Lanni, T., Drewnick, F., Demerjian, K. L., Kolb, C. E., and Worsnop, D. R.: Chase Studies of Particulate Emissions from in-use New York City Vehicles, Aerosol Sci. Tech., 38, 555-573, 10.1080/02786820490465504, 2004.

Gong, Z., Lan, Z., Xue, L., Zeng, L., He, L., and Huang, X.: Characterization of submicron aerosols in the urban outflow of the central Pearl River Delta region of China, Front. Environ. Sci. Eng., 725-733, 2012.

Gong, Z., Xue, L., Sun, T., Deng, Y., He, L., and Huang, X.: On-line measurement of PM_1 chemical composition and size distribution using a high-resolution aerosol mass spectrometer during 2011 Shenzhen Universiade, Scientia Sinica Chimica, 43, 363-372, 2013.

He, L. Y., Huang, X. F., Xue, L., Hu, M., Lin, Y., Zheng, J., Zhang, R., and Zhang, Y. H.: Submicron aerosol analysis and organic source apportionment in an urban atmosphere in Pearl River Delta of China using high-resolution aerosol mass spectrometry, J. Geophys. Res. Atmos., 116, 2011.

He, L. Y., Lin, Y., Huang, X. F., Guo, S., Xue, L., Su, Q., Hu, M., Luan, S. J., and Zhang, Y. H.: Characterization of high-resolution aerosol mass spectra of primary organic aerosol emissions from Chinese cooking and biomass burning, Atmos. Chem. Phys., 10, 11535-11543, 10.5194/acp-10-11535-2010, 2010.

Hu, W. W.: The sources and secondary formations of sub-micron organic aerosol in the typical atmospheric environments of China, Doctor of Philosophy, Peking University, Beijing, China, 2012.

Hu, W. W., Hu, M., Deng, Z. Q., Xiao, R., Kondo, Y., Takegawa, N., Zhao, Y. J., Guo, S., and Zhang, Y. H.: The characteristics and origins of carbonaceous aerosol at a rural site of PRD in summer of 2006, Atmos. Chem. Phys., 12, 1811-1822, 2012.

Hu, W. W., Hu, M., Yuan, B., Jimenez, J. L., Tang, Q., Peng, J. F., Hu, W., Shao, M., Wang, M., Zeng, L. M., Wu, Y. S., Gong, Z. H., Huang, X. F., and He, L. Y.: Insights on organic aerosol aging and the influence of coal combustion at a regional receptor site of central eastern China, Atmos. Chem. Phys., 13, 10095-10112, 2013.

Hu, W. W., Hu, M., Hu, W., Jimenez, J. L., Yuan, B., Chen, W., Wang, M., Wu, Y., Chen, C., Wang, Z., Peng, J., Yang, K., Zeng, L., and Shao, M.: Chemical composition, sources and aging process of sub-micron aerosols in Beijing: contrast between summer and winter. J. Geophys. Res. Atmos., doi: 10.1002/2015JD024020, 2016.

Huang, X. F., He, L. Y., Hu, M., Canagaratna, M. R., Kroll, J. H., Ng, N. L., Zhang, Y. H., Lin, Y., Xue, L., Sun, T. L., Liu, X. G., Shao, M., Jayne, J. T., and Worsnop, D. R.: Characterization of submicron aerosols at a rural site in Pearl River Delta of China using an Aerodyne High-Resolution Aerosol Mass Spectrometer, Atmos. Chem. Phys., 11, 1865-1877, 2011.

Huang, X. F., He, L. Y., Hu, M., Canagaratna, M. R., Sun, Y., Zhang, Q., Zhu, T., Xue, L., Zeng, L. W., Liu, X. G., Zhang, Y. H., Jayne, J. T., Ng, N. L., and Worsnop, D. R.: Highly time-resolved chemical characterization of atmospheric submicron particles during 2008 Beijing Olympic Games using an Aerodyne High-Resolution Aerosol Mass Spectrometer, Atmos. Chem. Phys., 10, 8933-8945, 2010.

Huang, X. F., He, L. Y., Xue, L., Sun, T. L., Zeng, L. W., Gong, Z. H., Hu, M., and Zhu, T.: Highly time-resolved chemical characterization of atmospheric fine particles during 2010 Shanghai World Expo, Atmos. Chem. Phys., 12, 4897-4907, 2012.

Huang, X. F., Xue, L., Tian, X. D., Shao, W. W., Sun, T. L., Gong, Z. H., Ju, W. W., Jiang, B., Hu, M., and He, L. Y.: Highly time-resolved carbonaceous aerosol characterization in

Yangtze River Delta of China: Composition, mixing state and secondary formation, Atmos. Environ., 64, 200-207, 2013.

Lanz, V. A., Alfarra, M. R., Baltensperger, U., Buchmann, B., Hueglin, C., Szidat, S., Wehrli, M. N., Wacker, L., Weimer, S., Caseiro, A., Puxbaum, H., and Prevot, A. S. H.: Source attribution of submicron organic aerosols during wintertime inversions by advanced factor analysis of aerosol mass spectra, Environ. Sci. Tech., 42, 214-220, 2008.

Li, W., and Shao, L.: Mixing and water-soluble characteristics of particulate organic compounds in individual urban aerosol particles, J. Geophys. Res. Atmos., 115, 2010.

Mohr, C., Huffman, J. A., Cubison, M. J., Aiken, A. C., Docherty, K. S., Kimmel, J. R., Ulbrich, I. M., Hannigan, M., and Jimenez, J. L.: Characterization of primary organic aerosol emissions from meat cooking, trash burning, and motor vehicles with high-resolution aerosol mass spectrometry and comparison with ambient and chamber observations, Environ. Sci. Tech., 43, 2443-2449, 2009.

Ng, N. L., Canagaratna, M. R., Zhang, Q., Jimenez, J. L., Tian, J., Ulbrich, I. M., Kroll, J. H., Docherty, K. S., Chhabra, P. S., Bahreini, R., Murphy, S. M., Seinfeld, J. H., Hildebrandt, L., Donahue, N. M., DeCarlo, P. F., Lanz, V. A., Prévôt, A. S. H., Dinar, E., Rudich, Y., and Worsnop, D. R.: Organic aerosol components observed in Northern Hemispheric datasets from Aerosol Mass Spectrometry, Atmos. Chem. Phys., 10, 4625-4641, 10.5194/acp-10-4625-2010, 2010.

Pathak, R. K., Wang, T., and Wu, W. S.: Nighttime enhancement of $PM_{2.5}$ nitrate in ammonia-poor atmospheric conditions in Beijing and Shanghai Plausible contributions of heterogeneous hydrolysis of N_2O_5 and HNO_3 partitioning, Atmos. Environ., 45, 1183-1191, 2011.

Xiao, R., Takegawa, N., Zheng, M., Kondo, Y., Miyazaki, Y., Miyakawa, T., Hu, M., Shao, M., Zeng, L., Gong, Y., Lu, K., Deng, Z., Zhao, Y., Zhang, Y. H.: Characterization and source apportionment of submicron aerosol with aerosol mass spectrometer during the PRIDE-PRD 2006 campaign. Atmos. Chem. Phys. 11, 6911-6929, 2011.

Ueda, S., Osada, K., and Takami, A.: Morphological features of soot-containing particles internally mixed with water-soluble materials in continental outflow observed at Cape Hedo, Okinawa, Japan, J. Geophys. Res. Atmos., 116, 2011.

Weimer, S., Alfarra, M. R., Schreiber, D., Mohr, M., Prévôt, A. S. H., and Baltensperger, U.: Organic aerosol mass spectral signatures from wood-burning emissions: Influence of burning conditions and wood type, J. Geophys. Res. Atmos., 113, 10.1029/2007jd009309, 2008.

Zhang, Q., Alfarra, M. R., Worsnop, D. R., Allan, J. D., Coe, H., Canagaratna, M. R., and Jimenez, J. L.: Deconvolution and quantification of hydrocarbon-like and oxygenated organic aerosols based on aerosol mass spectrometry, Environ. Sci. Tech., 39, 4938-4952, 2005.